Supplementary information for

Sulfamethoxazole degradation by Fe(II)-activated persulfate process : Insight into the reactive sites, products identification and degradation pathways

Ting Luo[a], Jinquan Wan[a, b, c, *], Yongwen Ma [a, b, c], Yan Wang [a, c], YongJie Wan[a]

[a] School of Environment and Energy, South China University of Technology, Guangzhou 510006, China

[b] Sino-Singapore International Joint Research Institute, Guangzhou 510006, China

[c] Guangdong Plant Fiber High-Valued Cleaning Utilization Engineering Technology Research Center, Guangzhou 510640, China

*** Corresponding Author:**

Jinquan Wan (Prof.)

E-mail: ppjqwan@scut.edu.cn

Summary:

Number of pages: 46

Number of tables: 8

Number of figures: 24

Supporting information Page

Text S1. Details of all chemicals used in this study

Sulfamethoxazole(SMX，$C_{10}H_{11}N_3O_3S$，98%，CAS 723-46-6) was obtained from Macklin Biochemical Co., Ltd. (Shanghai, China).Iron(II) sulfate heptahydrate($FeSO_4·7H_2O$，99%-101.0%) was purchased from Kemiou Chemical Reagent Co., Ltd.(Tianjin, China).Sodium persulfate($Na_2S_2O_8$, ≥98.0%) and formic acid(HCOOH, ≥88.0%) was obtained from Damao Chemical Reagent Factory (Tianjin, China). The analytical grades of humic acid(HA), sodium salt was purchased from Aladdin Chemistry Co., Ltd.(Shanghai, China). The analytical grades of methanol (MeOH) and tert-butanol (TBA) were obtained from Baishi Chemical Industry Co., Ltd.(Tianjin, China).Acetonitrile (ACN) and menthol were HPLC grade and obtained from RCI Labscan Limited (Thailand). Sodium chloride (NaCl, 99.5%), sodium bicarbonate ($NaHCO_3$, 99.5%), sodium nitrate ($NaNO_3$, 99.0%), and other chemicals used were purchased from Sinopharm Chemical Reagent Co., Ltd (Beijing, China).

Text S2. Details of HPLC system

The concentration of sulfamethoxazole was determined by HPLC system from Shimadu(Kyoto,Japan), equipped with a LC-20AT quaternary pump, a DGU-20A5 on-line degasser, a SIL-20A auto-sampler, and a SPD-20A photodiode array detector. Analytical separation was performed by a RP Hypersil BDS C18 column(5.0 μm particle size, 250 mm × 4.6 mm i.d.). Injection volume was set 20 μL by auto injector. UV detection was performed at 275 nm, and the column temperature was 28℃. The isocratic eluent consisted of 30% ACN and 70% H2O (with 0.2% formic acid) with a flow rate of 1.0 mL min−1. Quantification of the analytes was based on multipoint standard calibration curves with linear correlation coefficient (R2) values greater than 0.999.

Text S3. Details of UHPLC-HRMS/MS system

The degradation intermediates of sulfamethoxazole were identified by UHPLC-HRMS/MS techniques. Chromatography was accomplished on a VanquishTM Flex Binary UHPLC System (Thermo Fisher Scientific, Bremen, Germany). The UHPLC system consists of a binary pump with vacuum degasser, an autosampler, detector DAD and a column compartment. A Kinetex XB-C18 100A column (100 × 4.6 mm, 2.6 μm, Phenomenex Inc., Torrance, CA, USA) was used for separation. The binary mobile phase consisted of solvent A (99.8% H2O/0.2% formic acid) and solvent B (100% ACN). The chromatographic elution condition was as follows: 0–2 min, isocratic at 5% B; 2–8 min, gradient 5% to 35% B; 8–10 min, isocratic at 35% B; 10–10.1 min, gradient 35% to 5% B;10.1-12 min, isocratic at 5% B. The column compartment was kept at 25 °C, the flow rate was set at 0.3 mL/min, the injection amount was 10 μL and peaks were monitored at 275 nm.

A Q ExactiveTM Plus Hybrid Quadrupole-OrbitrapTM mass spectrometer (Thermo Fisher Scientific, Bremen, Germany) was coupled to the UHPLC system for detection. Ionization was achieved using a heated electrospray ionization source (HESI-II) in positive ionization mode (ESI+). Mass spectrometry data was collected using Full-MS/dd-MS2 (TopN = 10) method. Full mass scans were performed at a resolution of 70000 over the 50–600 m/z scan range. The automatic gain control (AGC) target and maximum injection time (IT) were set to 3 × 106 and 100 ms, respectively. The precursor ions filtered by the quadrupole in a 4.0 m/z isolation window were fragmented in the higher-energy collisional dissociation (HCD) collision cell with a

normalized collision energy (NCE) of 30. Product ions were detected in the Orbitrap mass analyzer at an AGC value of 1 × 105 and an IT of 50 ms. The mass spectrometry data were processed using Qual Browser Xcalibur 4.0 (Thermo Fisher Scientific).

Text S4. Details of effects of Fe(II) and PS concentration on SMX degradation

As shown in Fig.1, the SMX removal efficiency was 47% after 240min at a Fe(II):PS ratio of 1:1. An increase of Fe(II) concentration is not favorable for SMX degradation. Excess Fe(II) can significantly scavenge $SO_4^{\cdot-}$ (Eq.(3)), which otherwise participate in the SMX degradation. With the increase of PS concentration, the removal efficiency of SMX showed a trend of increasing first and then decreasing. Increasing the concentration of PS accelerates the consumption of Fe(II), thereby generating more sulfate radicals and improving the removal efficiency(Eq.(1)). However, the surplus of PS will reacts with the ROSs(Eqs.(4) and (5)), resulting in inhibition of SMX degradation. Note that, although secondary radicals of persulfate radical ($S_2O_8^{\cdot-}$) is generated , their lower oxidation potential precludes them playing an important role. In addition, sulfate radicals will themselves quench(Eq.(2)) ,resulting in reduced effective utilization of sulfate radicals.

$$Fe^{2+} + S_2O_8^{2-} \rightarrow Fe^{3+} + SO_4^{2-} + SO_4^{\cdot-} \quad (1)$$

$$SO_4^{\cdot-} + SO_4^{\cdot-} \rightarrow 2SO_4^{2-} \quad (2)$$

$$SO_4^{\cdot-} + Fe^{2+} \rightarrow SO_4^{2-} + Fe^{3+} \quad (3)$$

$$SO_4^{\cdot-} + S_2O_8^{2-} \rightarrow SO_4^{2-} + S_2O_8^{\cdot-} \quad (4)$$

$$\cdot OH + S_2O_8^{2-} \rightarrow OH^- + S_2O_8^{\cdot-} \quad (5)$$

Text S5. The effect of SMX concentration in solution on degradation

The effect of target contaminant(SMX) concentration in solution on degradation was investigated. When the initial concentration of SMX was 5 mg/L and 10 mg/L, the degradation curves completely coincided as shown in Fig.S2. In this case, SMX has completely degraded within 10 min. As the initial concentration of SMX increased, it showed a stronger inhibitory effect on SMX degradation. As the initial concentration of SMX increases, more SMX molecules and intermediates could compete for a certain amount of oxidant to reduce the rate of degradation. The rate constant of SMX degradation was $2.86\times10-3\ \mu M^{-1}min^{-1}$ at an initial SMX concentration of 20 mg/L. When the initial SMX concentration was increased to 80 mg/L, the rate constant was reduced to $5.45\times10^{-5}\ \mu M^{-1}min^{-1}$ with the removal efficiency correspondingly reduced to 82% (Table S2). It illustrates the Fe(II)-activated PS system can effectively remove SMX at a high concentration of 80 mg/L. It should be noted that the concentration of SMX is amplified for research, and the concentration of SMX in the environment ranges from ng/L to μg/L(Baran et al., 2011).

References

Baran, W., Adamek, E., Ziemiańska, J., Sobczak, A., 2011. Effects of the presence of sulfonamides in the environment and their influence on human health. J. Hazard. Mater. 196, 1–15. https://doi.org/10.1016/j.jhazmat.2011.08.082

Table S1. The pH change of the entire reaction process

Time（min)	The pH change at different Fe(II):PS molar ratios					
	2:1	1:1	1:5	1:10	1:20	1:40
0	7.03	7.07	6.08	3.3	2.55	2.11
15	2.58	2.66	2.6	2.58	2.37	2.09
30	2.25	2.52	2.58	2.56	2.35	2.07
60	2.52	2.61	2.53	2.52	2.34	2.07
120	2.31	2.46	2.48	2.57	2.39	2.08
210	2.28	2.48	2.53	2.59	2.38	2.08
250	2.56	2.57	2.5	2.53	2.37	2.06

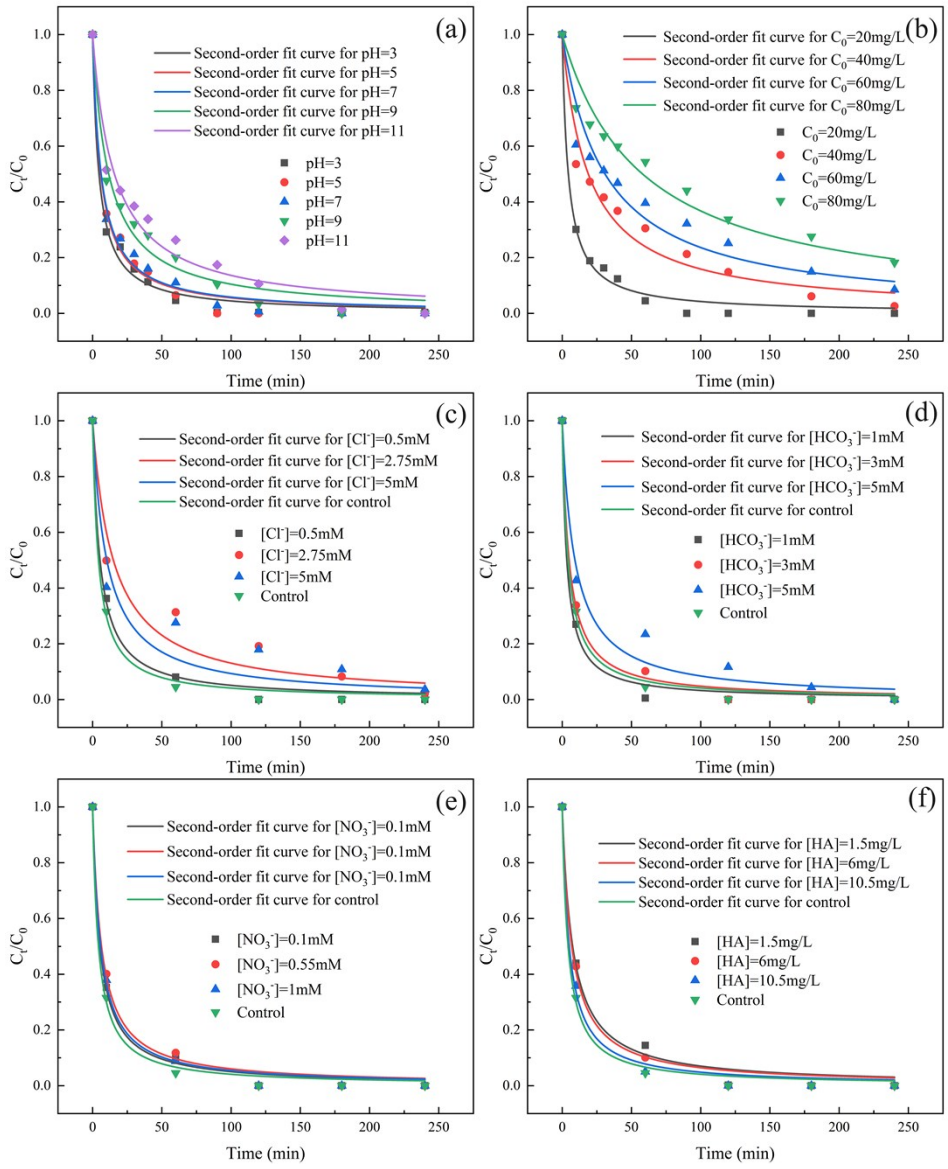

Fig.S1. Second-order fit curve of SMX degradation under different (a) pH;(b) SMX concentration;(c) Cl^- concentration;(d)HCO_3^- concentration;(e) NO_3^- concentration;(f) HA concentration. Experimental conditions: $[Fe^{2+}]_0$=2.5mM, $[PS]_0$=25mM, $[SMX]_0$=20mg/L, Temperature =25°C, initial pH without adjusted

Notes:

Model Second-order reaction kinetics

Equation $y=1/(1+k*C_0*x)$

C_0 represents the initial concentration of SMX, C_t represents the concentration of SMX at

reaction time t, and k is the second-order rate constant($\mu M^{-1}min^{-1}$).

Table S2. Second-order fit parameters of SMX degradation under different conditions.

		Rate constant($\mu M^{-1}min^{-1}$)	R^2	$t_{1/2}$(min)	Removal(%)
pH	3	2.73E-03	0.990	4.6	100
	5	2.16E-03	0.987	5.9	100
	7	2.05E-03	0.987	6.2	100
	9	1.09E-03	0.977	11.7	100
	11	8.04E-04	0.967	15.8	100
C_0(mg/L)	20	2.86E-03	0.992	4.4	100
	40	3.35E-04	0.963	18.9	97
	60	1.37E-04	0.942	30.9	92
	80	5.45E-05	0.954	58.0	82
Cl^-(mM)	0	2.96E-03	0.997	4.3	100
	0.5	2.37E-03	0.996	5.3	100
	2.75	8.44E-04	0.952	15.0	98
	5	1.23E-03	0.934	10.3	96
HCO_3^-(mM)	0	2.96E-03	0.997	4.3	100
	1	3.79E-03	0.995	3.3	100
	3	2.53E-03	0.996	5.0	100

	5	1.37E-03	0.977	9.2	100
NO_3^-(mM)	0	2.96E-03	0.997	4.3	100
	0.1	2.39E-03	0.996	5.3	100
	0.55	1.97E-03	0.994	6.4	100
	1	2.21E-03	0.995	5.7	100
HA(mg/L)	0	2.96E-03	0.997	4.3	100
	1.5	1.68E-03	0.995	7.5	100
	6	1.84E-03	0.993	6.9	100
	10.5	2.50E-03	0.991	5.1	100

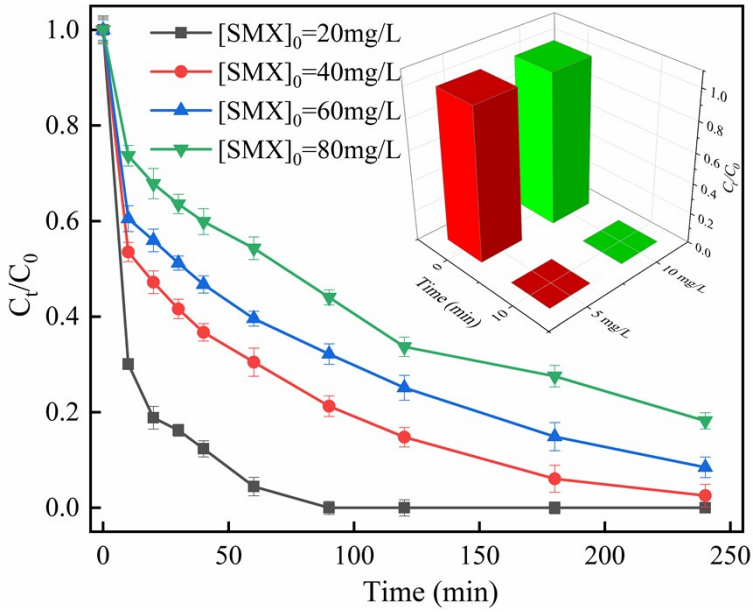

Fig.S2. Effect of the SMX concentration on SMX degradation. Experimental conditions: $[Fe^{2+}]_0$=2.5mM, $[PS]_0$=25mM, $[SMX]_0$=5-80mg/L, Temperature =25°C, initial pH without adjusted.

Table S3. TOC remaining in SMX solution

	TC(mg/L)	IC(mg/L)	TOC(mg/L)	removal extent
control	10.810	3.548	7.265	30%
treatment	9.603	4.514	5.089	

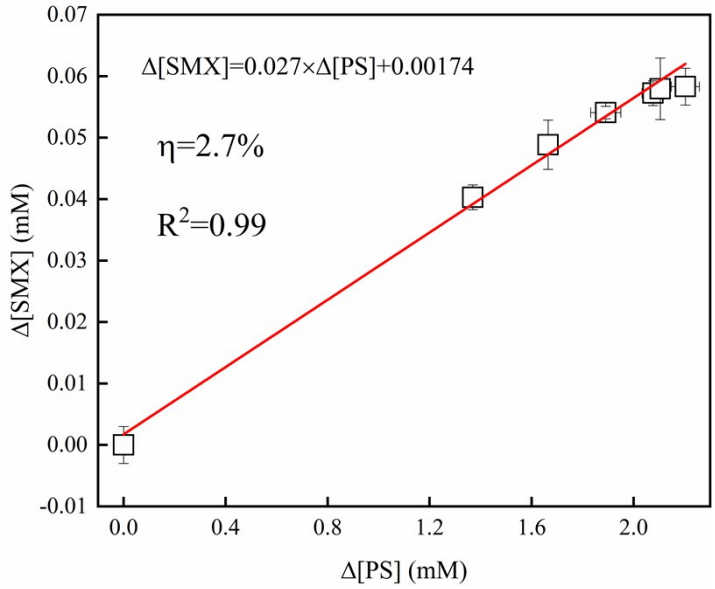

Fig.S3. Reaction stoichiometric efficiency of PS in Fe(II)-activated PS system.

Experimental conditions: $[Fe^{2+}]_0$=2.5mM, $[PS]_0$=25mM, $[SMX]_0$=20mg/L, Temperature =25°C, initial pH without adjusted.

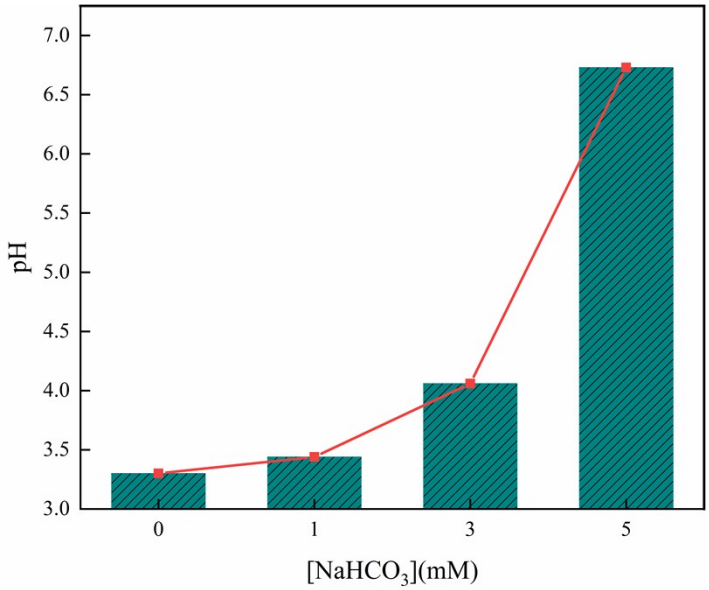

Fig.S4. The pH value after addition of bicarbonate. Experimental conditions: $[Fe^{2+}]_0$=2.5mM, $[PS]_0$=25mM, $[SMX]_0$=20mg/L,$[NaHCO_3]$=0-5mM, Temperature =25°C, initial pH without adjusted

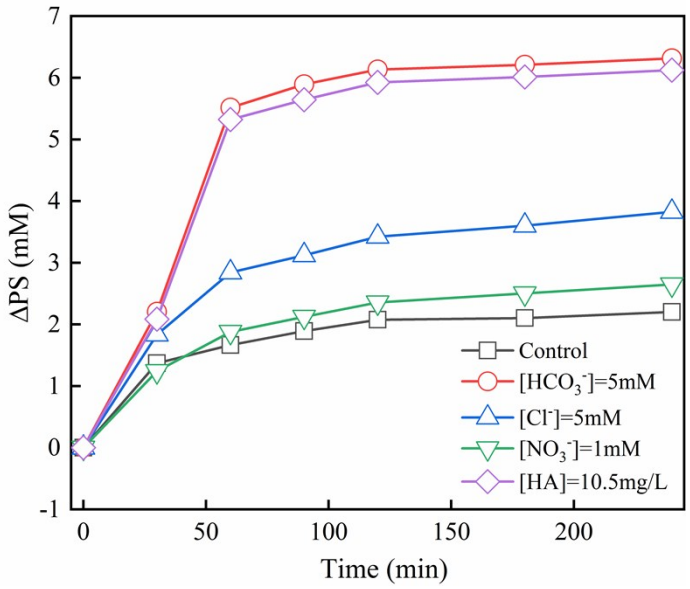

Fig.S5. The consumption of PS in the presence of different additives. Experimental conditions: $[Fe^{2+}]_0$=2.5mM, $[PS]_0$=25mM, $[SMX]_0$=20mg/L, Temperature =25°C, initial pH without adjusted.

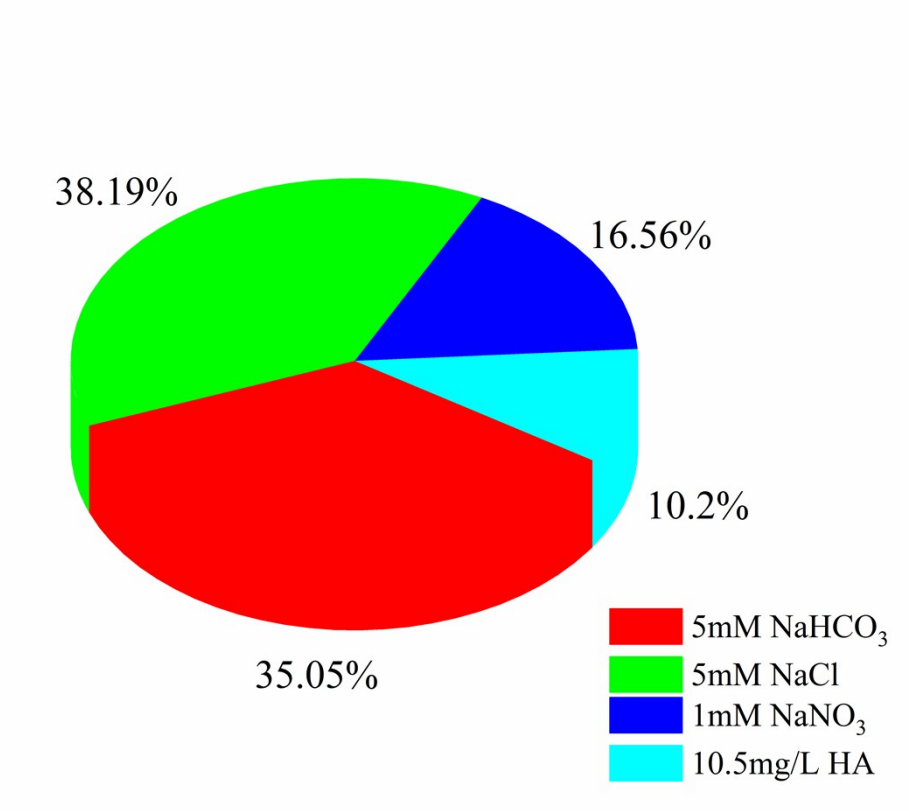

Fig.S6. The branching ratio of the scavenging effects. Experimental conditions:

$[Fe^{2+}]_0$=2.5mM, $[PS]_0$=25mM, $[SMX]_0$=20mg/L, Temperature =25°C, initial pH without adjusted.

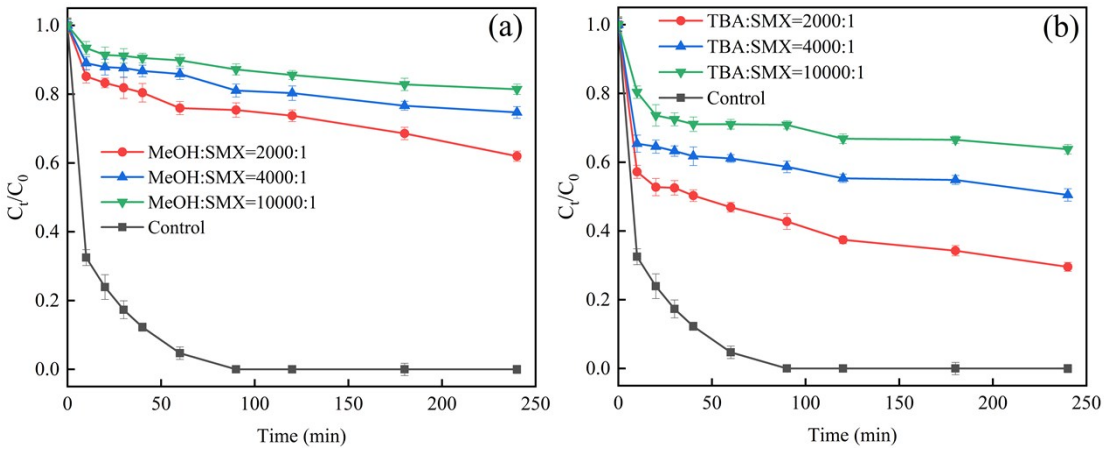

Fig.S7. Radical quenching studies: (a) Effects of MeOH;(b) Effects of TBA.

Experimental conditions: $[Fe^{2+}]_0$=2.5mM, $[PS]_0$=25mM, $[SMX]_0$=20mg/L, Temperature =25°C, initial pH without adjusted.

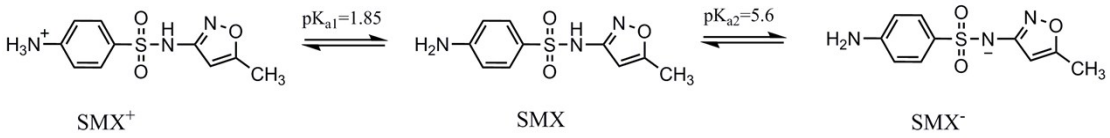

Notes:

SMX$^+$: cationic form

SMX: neutral form

SMX$^-$: anionic form

Fig.S8. Structure of SMX and its dissociation.

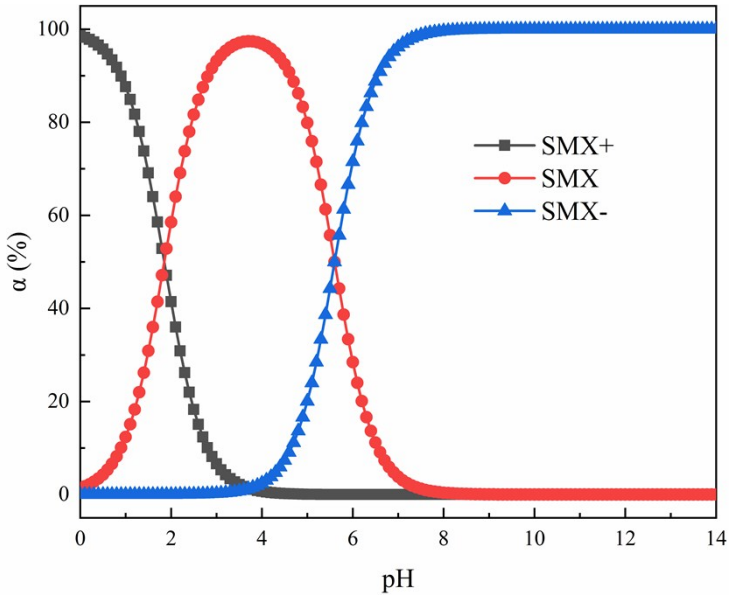

Fig.S9. Speciation diagram of SMX as a function of pH

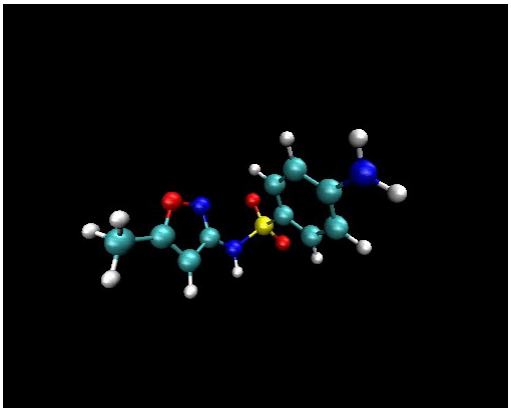

Fig.S10. Dynamic presentation of 243 conformations generated by the gentor program. (Double click to start the dynamic presentation)

Table S4. The three conformations of SMX optimized by MOPAC at the PM7 level

NO.	Count	E（a.u.)	DGmin	DE (kcal/mol)
1	54	-0.070767	0.30	0.00
2	162	-0.069243	0.30	0.96
3	27	-0.060988	2.40	6.14

Notes:

E: energy

DE: relative energy for the lowest energy conformation

DGmin: geometric deviation of the current conformation with its closest conformation, Count: number of identical structures (Energy threshold: 0.25kcal/mol ; geometric deviation: 0.25Angstrom)

Table S5. Energy Calculation at B3lyp/6-31G Level**

NO.	Thermal correction to Gibbs Free Energy(a.u.)	Single-point Energy (a.u.)	Solvation Free Energy (a.u.)	Solute Free Energy (a.u.)	Relative Energy (kcal/mol)
1	0.1645	-1175.9201	-0.0324	-1175.7850	0.0000
2	0.1641	-1175.9151	-0.0358	-1175.7838	0.7778
3	0.1636	-1175.9069	-0.0421	-1175.7823	1.6883

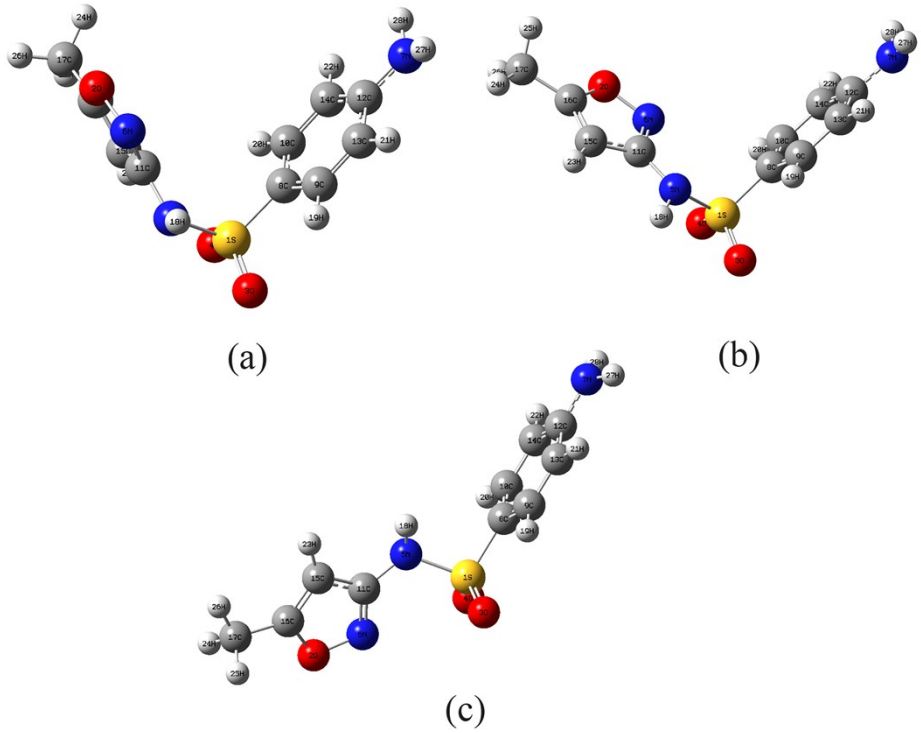

Fig.S11. The three conformations of SMX optimized by Gaussian at B3LYP/6-31G level**

Table S6. The percentage of Boltzmann distribution for each configuration

NO.	DE (kcal/mol)	Qi（Relat）	Percent (%)
1	0.0000	1.0000	75.38
2	0.7778	0.2688	20.27
3	1.6883	0.0577	4.35
Temperature: 298.15K		Q（Relat）：1.3266	

Notes:

Calculation formula : $p_i = \frac{e^{-\Delta E_i/RT}}{\sum_j e^{-\Delta E_j/RT}} = \frac{Q_{i(Relat)}}{Q_{(Relat)}}$

DE: relative energy for the lowest energy conformation

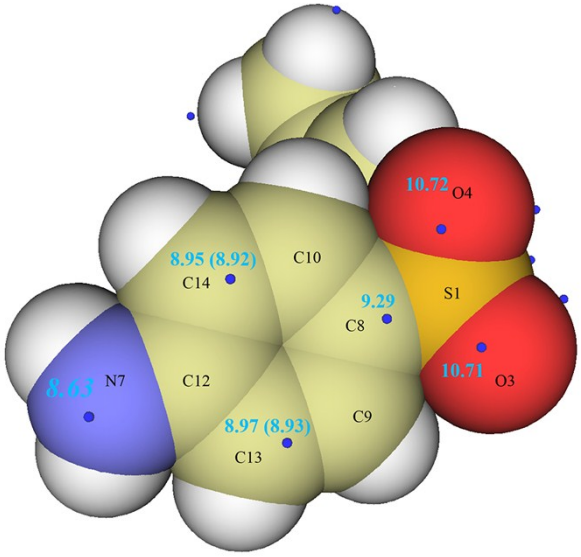

Fig.S12. Local minima of ALIE on vdW surface of SMX.

(The ALIE values (in eV) of the local minima involved in the aniline unit are labelled; the texts in the parentheses correspond to the ALIE values of the local minima at backside of the molecule. The global minimum of ALIE on the surface is labelled by italic font. The SMX structure is represented as superposition of vdW spheres.)

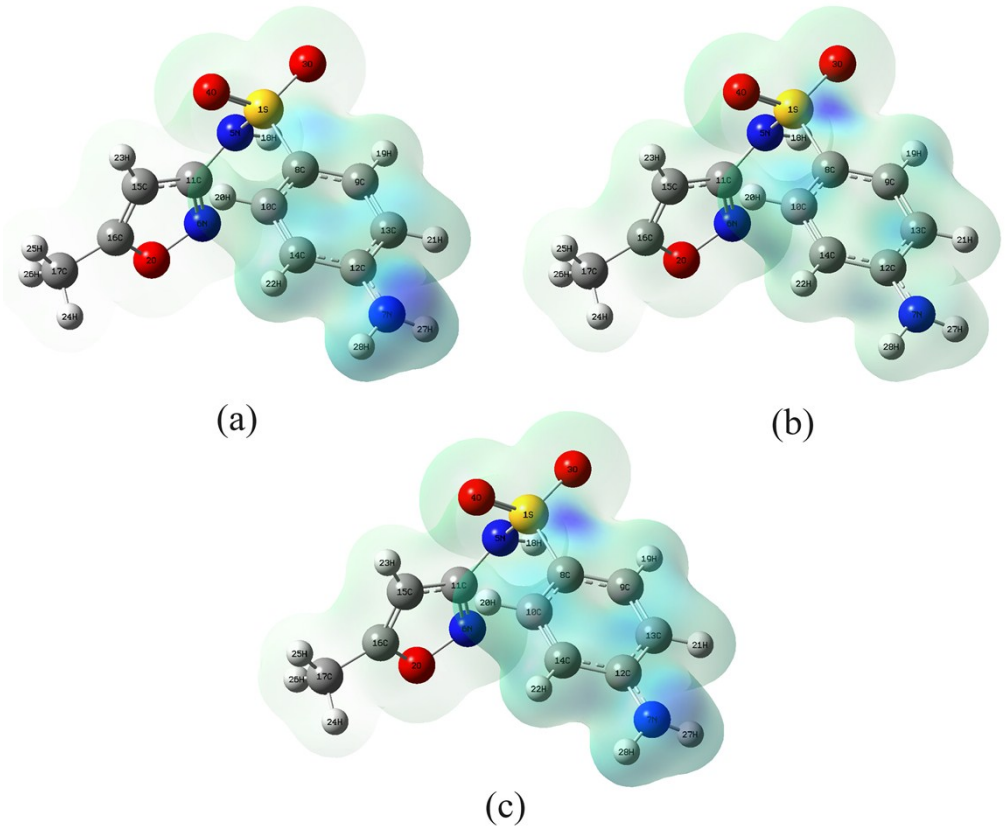

Fig.S13. The Fukui function mapped electron density isosurface (ρ=0.01 a.u.):(a) f-(r);(b) f+(r);(c) f0(r).

(The dark blue on the isosurface corresponds to the larger positive value of the Fukui function.)

Table S7. Condensed Fukui function and dual descriptor calculated by Hirshfeld population

	N	N-1	N+1	f-	f+	f0	Δf
1S	0.5123	0.5343	0.4385	0.0220	0.0738	0.0479	0.0519
2O	-0.0856	-0.0776	-0.1166	0.0080	0.0310	0.0195	0.0230
3O	-0.3759	-0.3480	-0.4248	0.0279	0.0489	0.0384	0.0210
4O	-0.3595	-0.3321	-0.4041	0.0275	0.0446	0.0360	0.0171
5N	-0.1268	-0.1022	-0.1569	0.0246	0.0300	0.0273	0.0054
6N	-0.1706	-0.1588	-0.2212	0.0118	0.0505	0.0312	0.0387
7N	-0.1372	0.0435	-0.1902	0.1806	0.0530	0.1168	-0.1276
8C	-0.0678	0.0229	-0.1256	0.0908	0.0578	0.0743	-0.0330
9C	-0.0317	0.0128	-0.0946	0.0445	0.0629	0.0537	0.0183
10C	-0.0338	0.0103	-0.1142	0.0441	0.0804	0.0623	0.0363
11C	0.0643	0.0678	0.0347	0.0036	0.0296	0.0166	0.0260
12C	0.0667	0.1369	-0.0165	0.0702	0.0833	0.0767	0.0131
13C	-0.0558	0.0345	-0.1016	0.0902	0.0459	0.0680	-0.0444
14C	-0.0567	0.0369	-0.1003	0.0937	0.0435	0.0686	-0.0501
15C	-0.0918	-0.0870	-0.1098	0.0047	0.0180	0.0114	0.0133
16C	0.0954	0.1001	0.0674	0.0047	0.0280	0.0164	0.0233
17C	-0.0657	-0.0640	-0.0742	0.0017	0.0085	0.0051	0.0069
18H	0.1516	0.1616	0.1346	0.0101	0.0170	0.0135	0.0069
19H	0.0578	0.0816	0.0284	0.0239	0.0294	0.0266	0.0055

20H	0.0542	0.0776	0.0190	0.0233	0.0352	0.0293	0.0119
21H	0.0598	0.0956	0.0355	0.0358	0.0243	0.0300	-0.0115
22H	0.0595	0.0962	0.0359	0.0367	0.0235	0.0301	-0.0132
23H	0.0623	0.0658	0.0503	0.0036	0.0120	0.0078	0.0084
24H	0.0585	0.0598	0.0503	0.0013	0.0082	0.0047	0.0069
25H	0.0614	0.0626	0.0561	0.0012	0.0053	0.0032	0.0041
26H	0.0585	0.0600	0.0508	0.0015	0.0078	0.0046	0.0063
27H	0.1483	0.2043	0.1243	0.0561	0.0240	0.0400	-0.0321
28H	0.1484	0.2044	0.1248	0.0561	0.0235	0.0398	-0.0325

Notes:

N:Hirshfeld charges for all atoms in SMX in its N electrons states

N-1:Hirshfeld charges for all atoms in SMX in its N-1 electrons states

N+1:Hirshfeld charges for all atoms in SMX in its N+1 electrons state

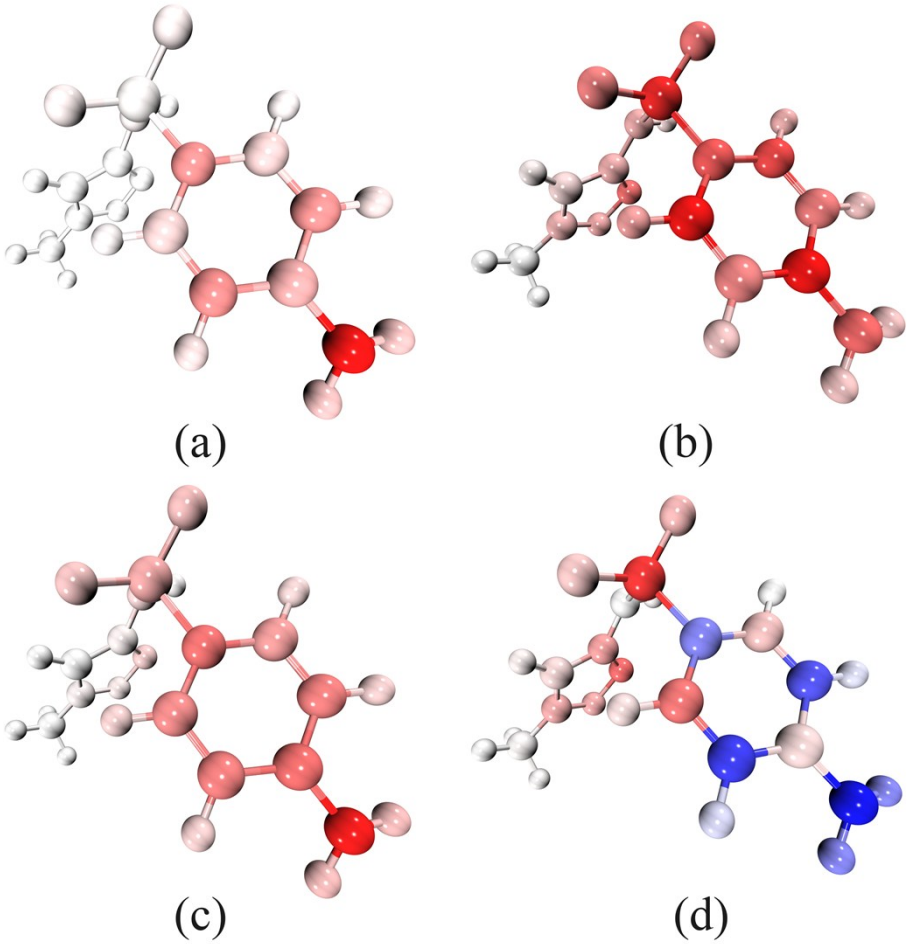

Fig.S14. Atomic coloring maps of condensed Fukui function and dual descriptor:

(a) f^-;(b) f^+;(c) f^0;(d) Δf.

(Red and blue correspond to positive and negative value, respectively.)

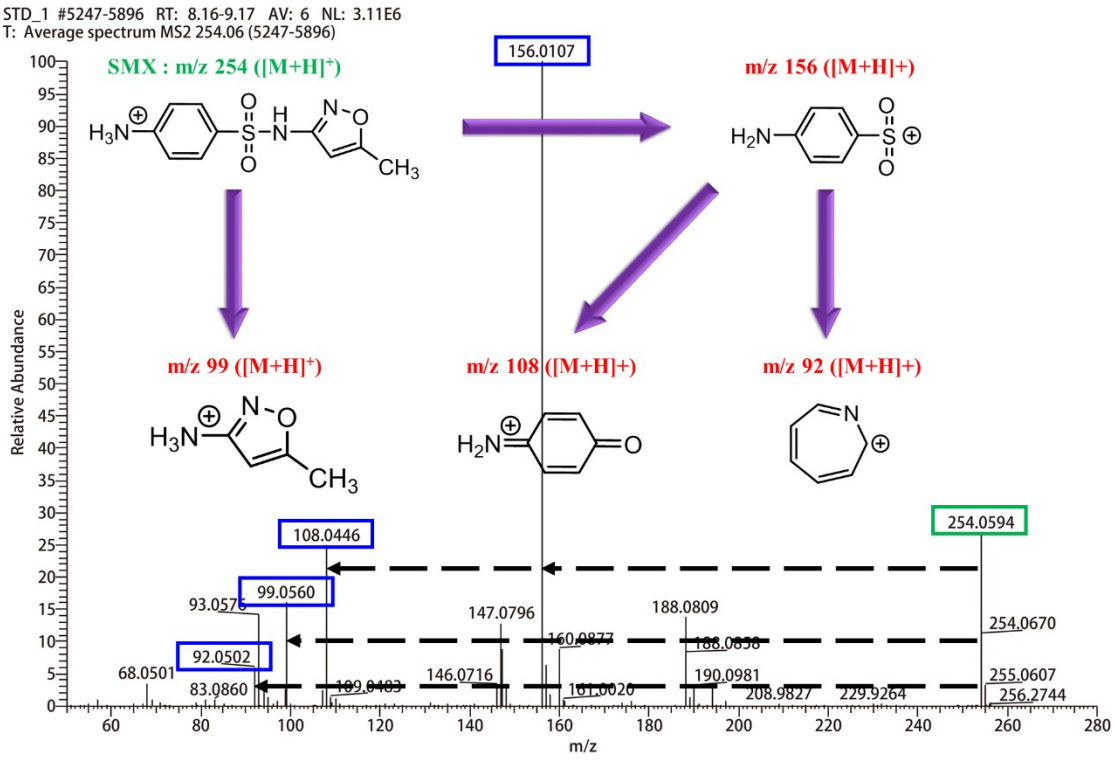

Fig.S15. Identification of SMX (m/z$^+$ 254)

Fragment ion 99,156, 108 and 92

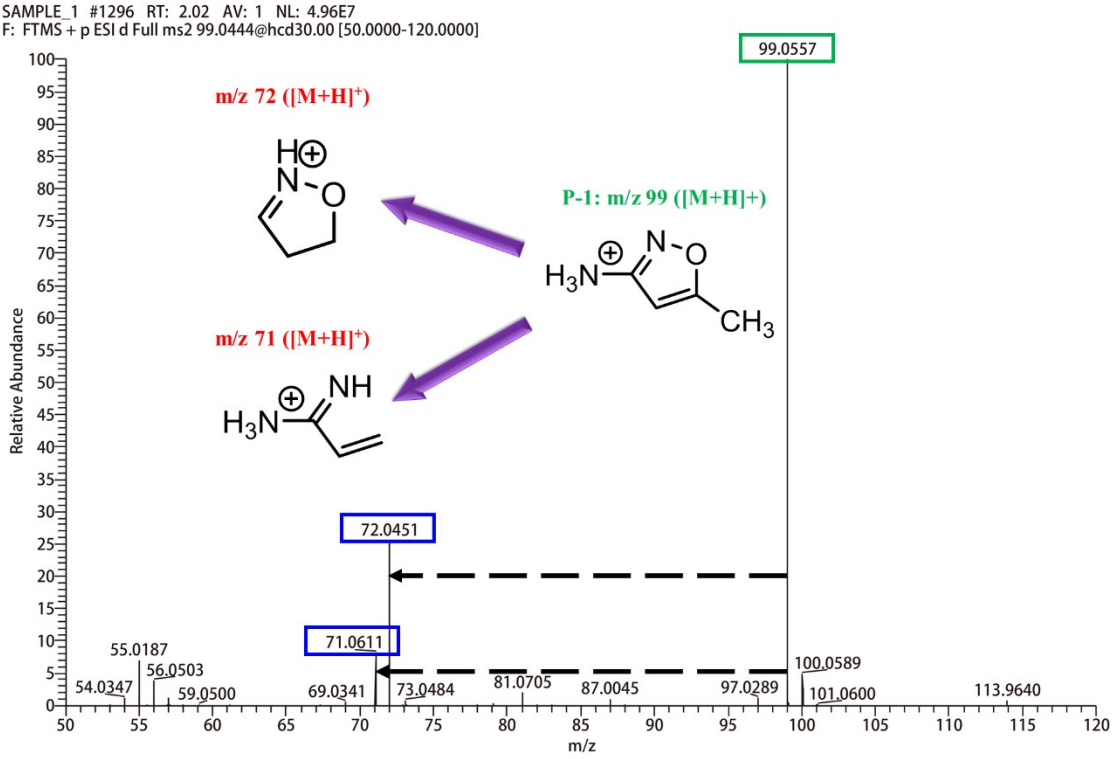

Fig.S16. Identification of P-1 (m/z^+ 99)

Fragment ion 72 and 71

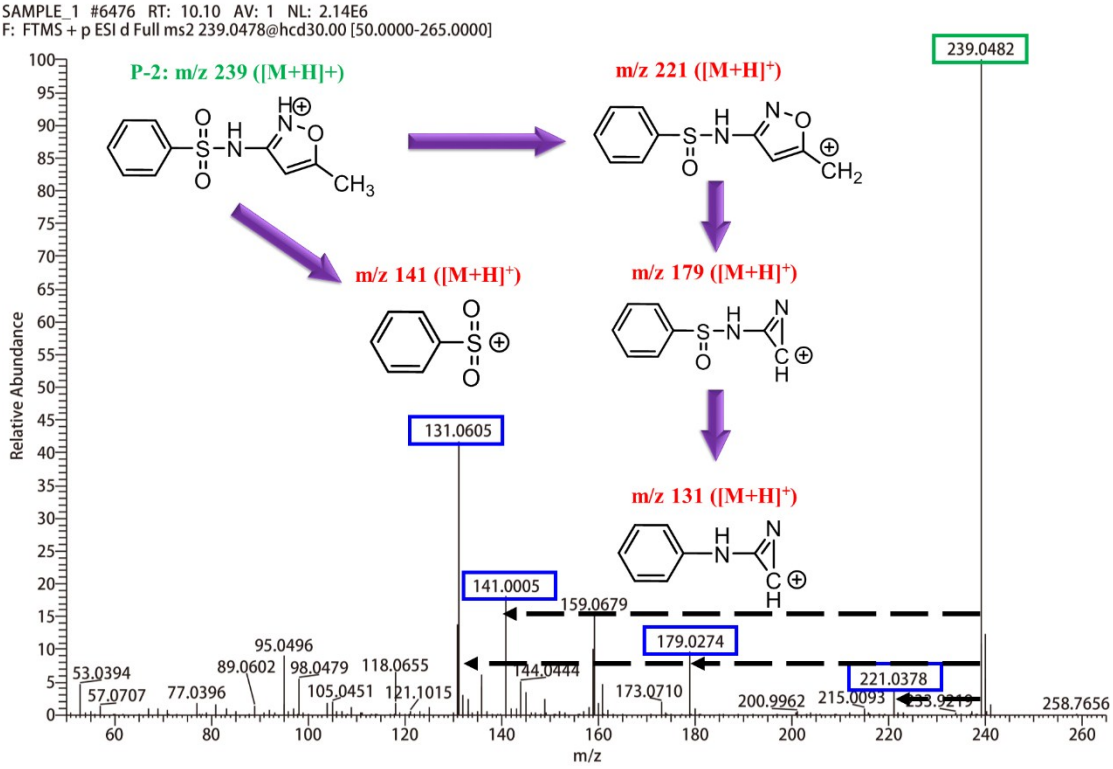

Fig.S17. Identification of P-2 (m/z+ 239)

Fragment ion 141,221,179 and 131

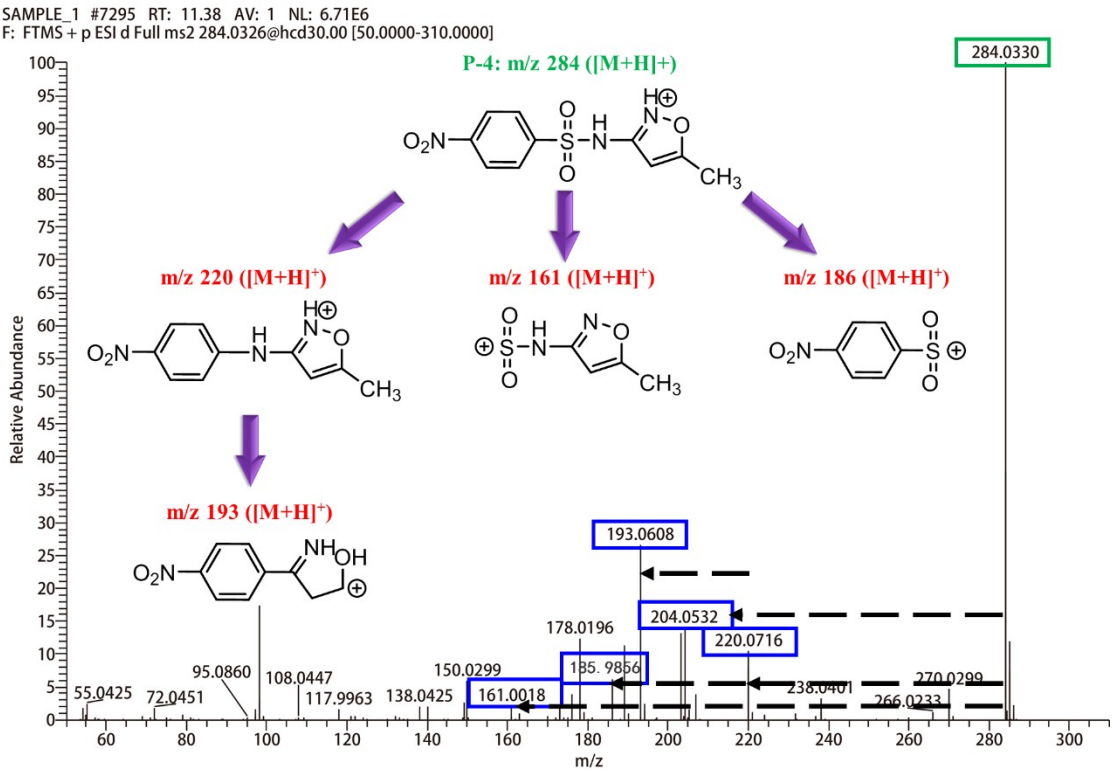

Fig.S18. Identification of P-3 (m/z^+ 284)

Fragment ion 220,161,186 and 193

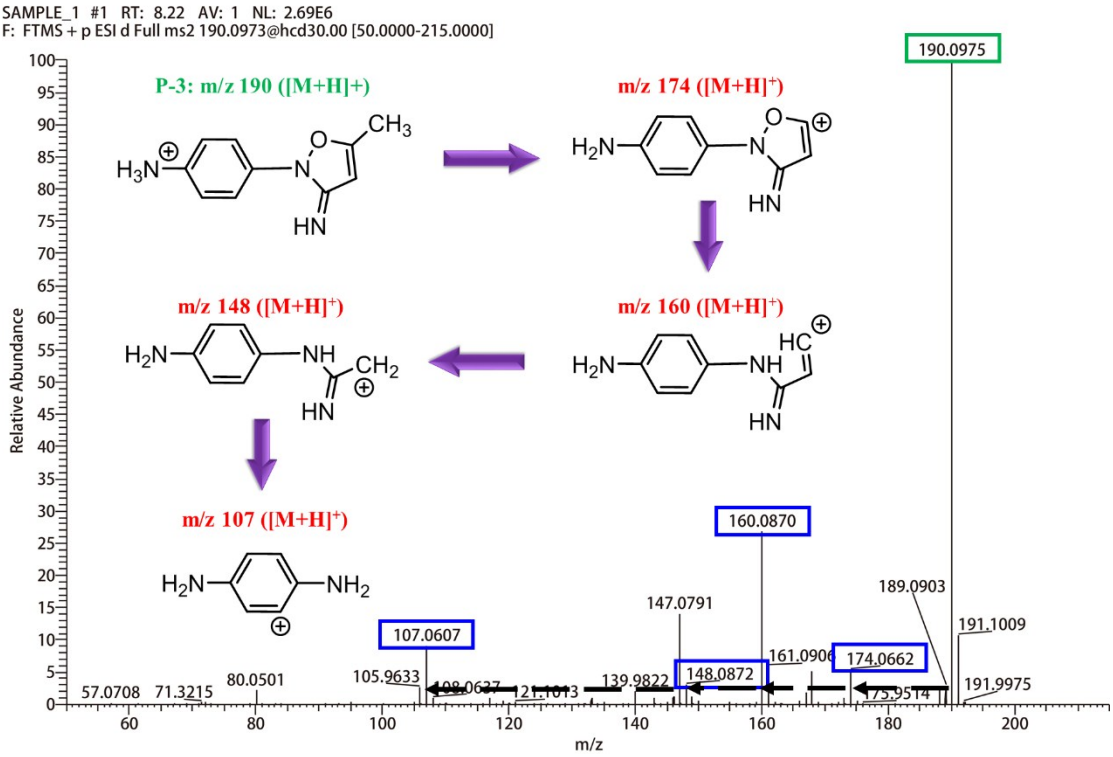

Fig.S19. Identification of P-4 (m/z^+ 190)

Fragment ion 174,160,148 and 107

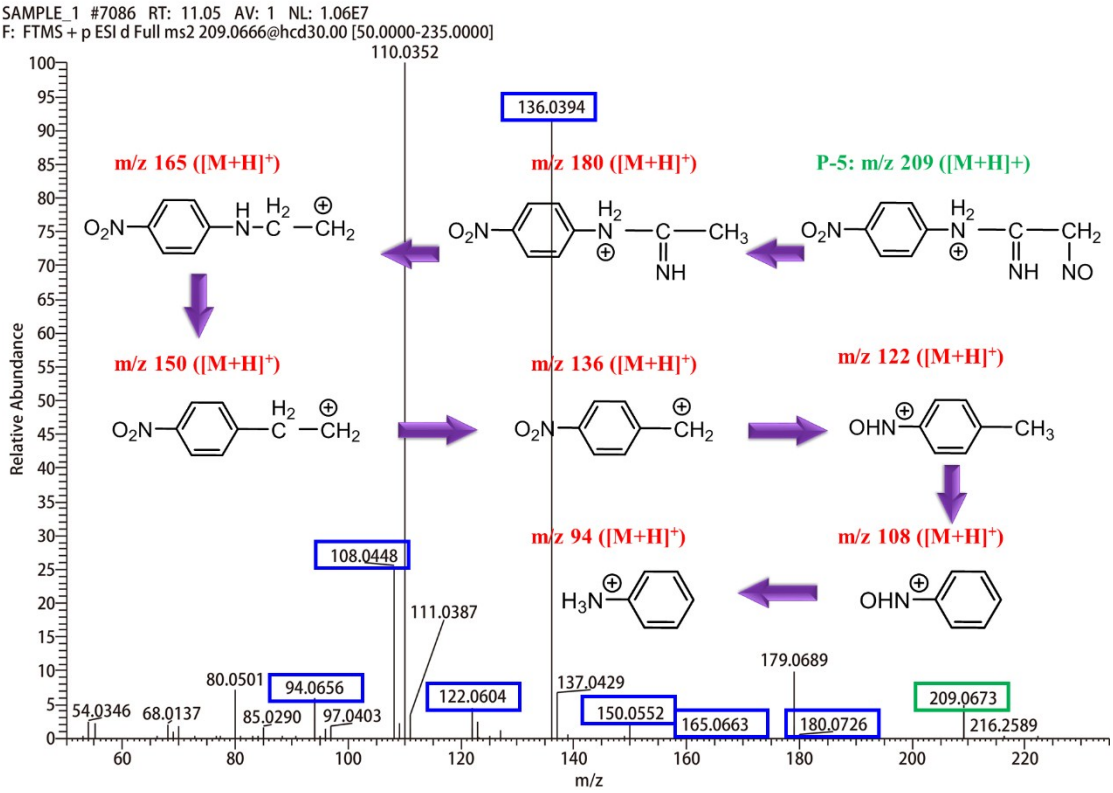

Fig.S20. Identification of P-5 (m/z$^+$ 209)

Fragment ion 180,165,150,136,122,108 and 94

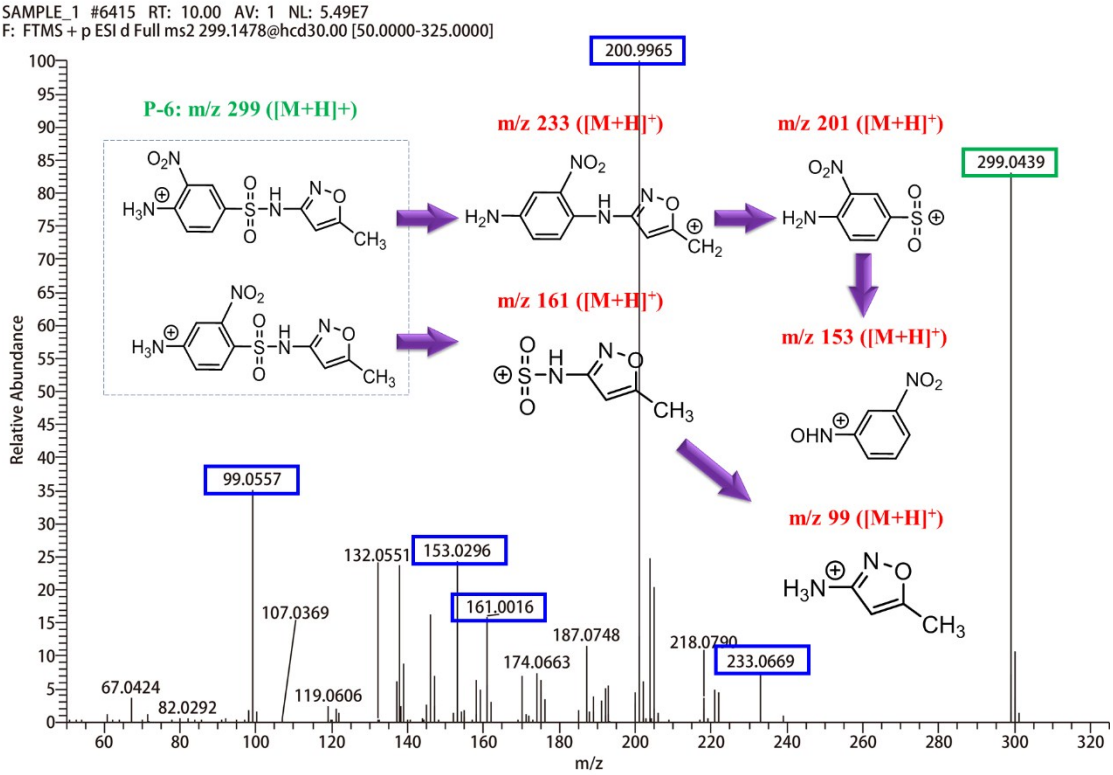

Fig.S21. Identification of P-6 (m/z^+ 299)

Fragment ion 233,201,153,99 and 161

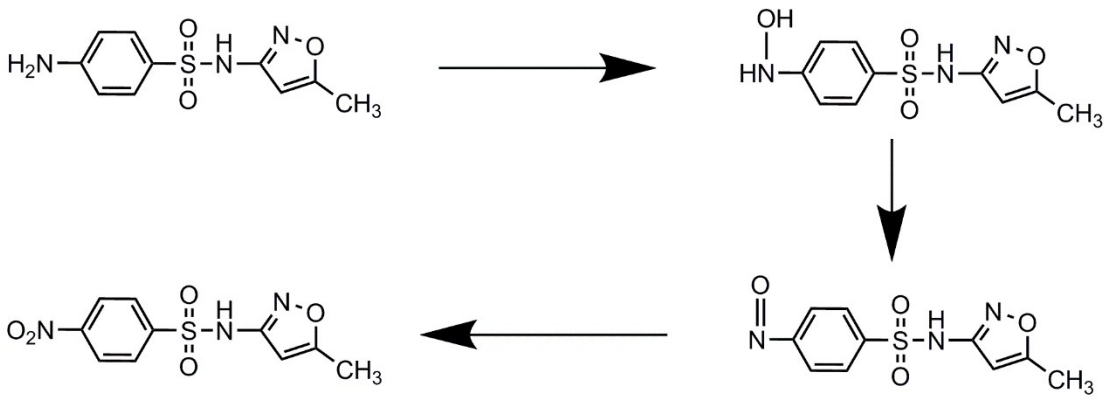

Figure S22. The formation mechanism of 4-nitro-SMX

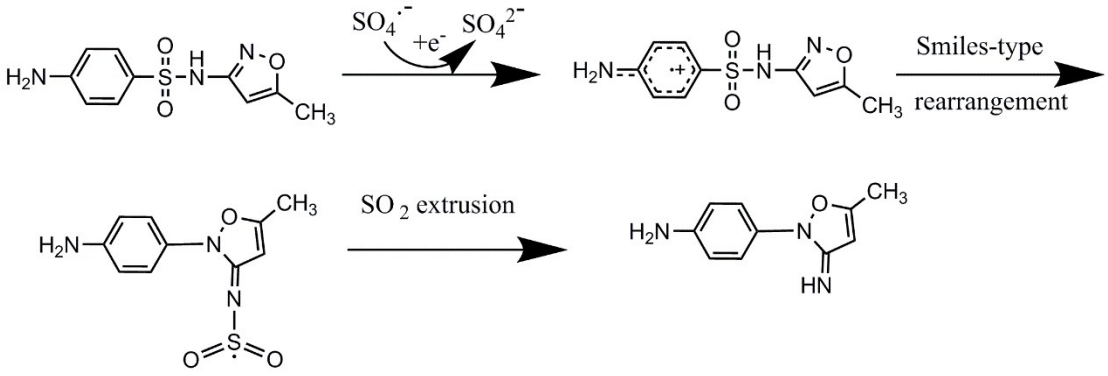

Figure S23. The formation mechanism of SEP

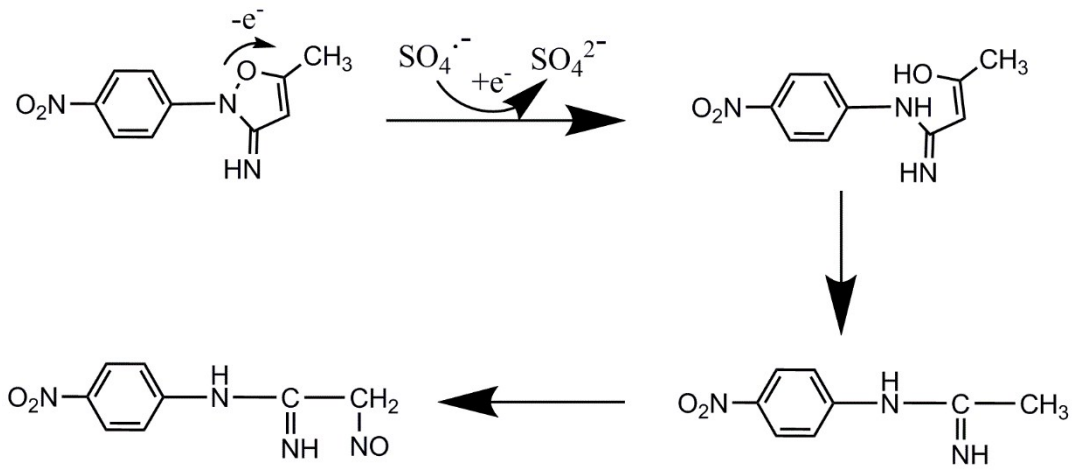

Figure S24. Cleavage pathway of the oxazole ring

Table S8. Retention times, fragments, accurate mass measurement for SMX and its products.

Compounds	Ion formula [M+H]+	Experimental mass(m/z)	Calculated mass(m/z)	Errorr (ppm)	DBE	Loss
SMX(RT:8.21min)	C10H12O3N3S	254.0594	254.0620	-0.15	6.5	-
FG1	C6H6N	92.0502	92.0510	7.54	4.5	C4H6N2O3S
FG2	C4H7ON2	99.0560	99.0570	6.87	2.5	C6H5O2NS
FG3	C6H6ON	108.0446	108.0460	1.66	4.5	C4H6N2O2S
FG4	C6H6O2NS	156.0107	156.0130	-4.50	4.5	C4H6N2O
P-1(RT:2.02min)	C4H7ON2	99.0556	99.0570	3.14	2.5	-
FG1	C3H6ON	72.0451	72.0460	9.43	1.5	CHN
FG2	C3H7N2	71.0611	71.0620	9.92	1.5	CO
P-2(RT:10.10min)	C10H11O3N2S	239.0479	239.0510	-2.30	6.5	-
FG1	C8H7N2	131.0605	131.0620	0.16	6.5	C2H4O3S
FG2	C6H5O2S	141.0005	141.0020	-0.03	4.5	C4H6ON2
FG3	C10H9O2N2S	221.0378	221.0400	-0.43	7.5	H2O
FG4	C8H7ON2S	179.0274	179.0290	0.05	6.5	C2H4O2
P-3(RT:11.38min)	C10H10O5N3S	284.0330	284.0360	-1.93	7.5	-
FG1	C4H5O3N2S	161.0018	161.00	1.62	3.5	C6H5O2N
FG2	C6H4O4NS	185.9856	185.99	0.46	5.5	C4H6ON2
FG3	C9H9O3N2	193.0608	193.0630	0.37	6.5	CHO2NS
FG4	C10H10O3N3	220.0716	220.0740	-0.49	7.5	O2S

P-4(RT:8.22min)	C10H12ON3	190.0975	190.1000	0.06	6.5	-
FG1	C6H7N2	107.0607	107.0620	3.41	4.5	C4H5ON
FG2	C8H10N3	148.0872	148.0890	2.07	5.5	C2H2O
FG3	C9H10N3	160.0870	160.0890	0.41	6.5	CH2O
FG4	C9H8ON3	174.0662	174.0680	0.30	7.5	CH4
P-5(RT:11.05min)	C8H9O3N4	209.0673	209.0690	-1.54	2.5	-
FG1	C8H10O2N3	180.0726	180.0790	-8.24	5.5	ON
FG2	C8H9O2N2	165.0663	165.0680	-1.75	1.5	ON2
FG3	C8H8O2N	150.0552	150.0570	1.70	5.5	ON3
FG4	C7H6O2N	136.0394	136.0410	0.92	5.5	CH3ON3
FG5	C7H8ON	122.0604	122.0620	2.86	4.5	CHO2N3
FG6	C6H6ON	108.0448	108.0460	3.42	4.5	C6H6ON
FG7	C6H8N	94.0656	94.0670	5.36	3.5	C2HO3N3
P-6(RT:10.00min)	C10H11O5N4S	299.0433	299.0470	-1.96	7.5	-
FG1	C4H7ON2	99.0558	99.0570	4.65	2.5	C6H4O4N2S
FG2	C6H5O3N2	153.0296	153.0310	0.60	5.5	C4H6O2N2S
FG3	C4H5O3N2S	161.0016	161.0030	0.32	3.5	C6H6O2N2
FG4	C6H5O4N2S	200.9965	200.9980	0.43	5.5	C4H6ON2
FG5	C10H9O3N4	233.0669	233.0690	0.10	8.5	H2O2S